Building 1D and 3D static reservoir geomechanical properties models in the oil field

Manouchehr Sanei[1] · **Ahmad Ramezanzadeh**[2] · **Amin Asgari**[2]

Abstract

Reservoir geomechanical models provide valuable information for various applications ranging from the prediction of surface subsidence to the determination of pore pressure and induced stress changes, wellbore stability, fault reactivation, and caprock integrity. Three-dimensional geological modeling of reservoir geomechanics is an essential tool to predict reservoir performance by considering the geomechanics effects. Thus, this study focuses on the application of 3D static reservoir geomechanical model workflow by using 3-D seismic and well log data for proper optimization in the Volve oil field, Norway. 3D Seismic data are applied to generate the interpreted horizon grids and fault polygons. The horizon which cut across the nine wells is used for the detailed topographic analysis. The workflow includes 1D geomechanical and petrophysical models which are calculated at well locations by using log data. Structural and property modeling (pore pressure, vertical and horizontal stresses, elastic properties, porosity, permeability, and hydrocarbon saturation) is distributed by geostatistical methods such as Kriging and Gaussian. This study indicates the effectiveness of the three-dimensional static modeling technique as a tool for better understanding of the spatial distribution of reservoir geomechanical properties, hence, providing a framework for analyzing future activities in the reservoir such as proposal position and trajectory of new wells for future field development and assessing arbitrary injection-production schedules.

Keywords Reservoir geomechanical modeling · Well logging data · Geostatistical methods · Volve oil field

List of symbols

1D	One-dimensional
3D	Three-dimensional
A	Regression coefficient
a	Archie factor
B	Regression coefficient
c	Constant
DT	Compressional sonic transit time $[\mu s/\text{ft}]$
DT_{ml}	Mudline transit time $[\mu s/\text{ft}]$
DT_n	Sonic transit time on the normal line
DT_{sh}	Compressional transit time in shale
E	Young modulus $[\text{Gpa}]$
E_d	Dynamic Young modulus $[\text{Gpa}]$
E_s	Static Young modulus $[\text{Gpa}]$
F	Fracture reopening
g	Gravitational acceleration $[\text{m/s}^2]$
k	Coefficient of earth's stress
k	Permeability
m	Cementation exponent
ml	Multiplier
n	Saturation exponent
p_{hyd}	Hydrostatic pressure $[\text{Mpa}]$
p_p	Pore pressure $[\text{Mpa}]$
R_t	True resistivity $[\Omega\,\text{m}]$
R_w	Resistivity of formation water $[\Omega\,\text{m}]$
SGS	Sequential Gaussian simulation
S_h	Hydrocarbon saturation
S_{tec}	Tectonic stress $[\text{Mpa}]$
S_v	Vertical stress $[\text{Mpa}]$
S_v	Overburden stress $[\text{Mpa}]$
S_w	Water saturation
TVD	True vertical depth $[\text{m}]$
V_p	Compressional wave velocity $\left[\frac{\text{km}}{\text{s}}\right]$
VSH	Shale volume
V_s	Shear wave velocity $\left[\frac{\text{km}}{\text{s}}\right]$
UCS	Unconfined compressive strength $[\text{Gpa}]$
z	Depth

✉ Manouchehr Sanei
  manouchehr.sanei@gmail.com

1 Yazd University, Yazd, Iran

2 Shahrood University of Technology, Shahroud, Iran

α	Biot's coefficient
ε_x	Strain in the x direction
ε_y	Strain in the y direction
ν	Poisson's ratio
ν_d	Dynamic Poisson ratio [%]
ν_s	Static Poisson ratio
ρ	Bulk density of the formation [g/cm^3]
ρ_b	Measured bulk density (RHOB) [g/cm^3]
ρ_{fl}	Fluid density [g/cm^3]
ρ_{ma}	Matrix density [g/cm^3]
ρ_w	Density of water
$\rho(z)$	Bulk density [g/cm^3]
ϕ	Total porosity

Introduction

A comprehensive understanding of the stress state and fluid-rock interaction conditions in porous media prior to various scenarios such as drilling, stimulation, and production of hydrocarbon reservoirs plays a very important role in predicting their safe and economical operation. Subsurface stresses and their interaction with reservoir pore pressure affect a variety of operational aspects such as wellbore stability, wellbore integrity, caprock integrity, fault reactivation, early water-cut, sand production, pore collapse, reservoir compression, surface subsidence, and water/gas flooding during an oil/gas field life as well as stimulation techniques such as hydraulic fracture and acid fracturing (Zoback et al. 1985; Koutsabeloulis et al. 2009; Herwanger 2011; Fischer and Henk 2013; Sanei et al. 2017; Duran et al. 2020; Sanei et al. 2021; Sanei et al. 2022).

In addition, as a result of improved living standards and the advancement of technology, the demand for energy in the world has increased. This has also led to many challenges related to the discovery of new fields (Osinowo et al. 2018). Hydrocarbon exploration is moving toward reservoirs with more complex geologies, thus systematic operations to increase and optimize oil production to meet energy demand are essential. Therefore, the development of an integrated approach that requires various sciences such as geology, geophysics, petrophysics, geostatistics, geomechanics, and reservoir engineering to describe the reservoirs and their properties is essential (Ma 2011; Yu et al. 2011; Osinowo et al. 2018; Ashraf et al. 2019; Jiang et al. 2021; Anees et al. 2022a; Mangi et al. 2022; Safaei et al. 2022).

The advances in computational and computer technology have made it possible for modern reservoir models to incorporate more accurate spatial distributions of reservoir properties. Subsurface reservoir characterization generally includes well log data augmented with seismic data to establish the geological model of the reservoir (Patrick et al. 2002). Reservoir characterization is a technique for quantifying the rock and fluid properties of a reservoir. This technique requires all the information needed to describe a reservoir (Chopra and Michelena 2011; Yu et al. 2011; Ashraf et al. 2020b; Anees et al. 2022b). Reservoir modeling is an essential step in field development because it provides a place to integrate all available data and geologic concepts (Branets et al. 2009).

The 3D static geological modeling of the reservoir contains a 3D structure of its volume (Chambers et al. 2000; Thanh et al. 2019; Thanh et al. 2022). A three-dimensional static model of the reservoir is a definition of the structure, stratigraphy, and rock properties at a special time (Thanh et al. 2020; Ashraf et al. 2021). One of the key challenges in reservoir modeling is the appropriate representation of reservoir geometry, including the structural framework and detailed stratigraphic layers (Novak et al. 2014). Various data such as well logging, cores, well testing, and production data are utilized to build the static reservoir model (Davis 2002). The built reservoir model comprises two stages of construction modeling and petrophysical modeling, in which the reservoir properties are distributed by the geostatistical methods in the structure of the reservoir (Flugel 2004). The geostatistical methods such as deterministic methods (such as Kriging) and stochastic (such as Sequential Gaussian Simulation) methods are generally applied in order to construct the reservoir model (Thanh et al. 2020; Thanh and Sugai 2021). The static reservoir geomechanical modeling consists of a reservoir model and a geomechanics model. As expressed, the static reservoir model can be constructed using geostatistical methods. In addition, the geomechanical properties model can be built similar to the static reservoir model by applying the geostatistical methods. Numerical modeling, especially the reservoir geomechanical model is a reliable tool that considers a variety of data such as geological, geophysical, and engineering data to be capable to analyze various scenarios throughout the life of the reservoir (Fischer et al. 2013; Henk 2009; Khaksar et al. 2012; Tenthorey et al. 2013; Guerra et al. 2019).

In conventional reservoir simulation, the only geomechanical parameter involved is rock compressibility. This parameter is not enough to indicate different rock behaviors such as stress path dependency, pore collapse, dilatancy (Gutierrex, M., and R.W. Lewis 1998; Pereira et al. 2008). To fundamentally represent these behaviors, especially in complex, heterogeneous, and unconventional reservoirs, a realistic 3D model of reservoir geomechanics is essential, which is very difficult to construct. When the numerical model of reservoir geomechanics has been built, it can be used as a prior tool for various future operational scenarios such as wellbore stability, optimal trajectory of drilling, caprock integrity, fault reactivation, pore collapse, surface subsidence, water/gas flooding in order to improve the safety

and economics of the projects (Bachmann et al. 1987; Khaksar et al. 2012; Sanei et al. 2021, 2022).

In this study, considering the importance of geomechanics in reservoirs, the numerical workflow of static reservoir geomechanical modeling is presented based on the data of the Volve oil field, which is a complex geological reservoir. This workflow consists of 1D geomechanical and reservoir modeling which are computed using well logging data. The 3D static reservoir geomechanical modeling comprises the 3D geomechanical properties, e.g., pore pressure, elastic properties, vertical stress, horizontal stresses, and 3D reservoir properties, e.g., porosity, permeability, and hydrocarbon saturation, which are constructed using geostatistical methods such as Kriging and Sequential Gaussian Simulation method. This three-dimensional static reservoir geomechanical modeling provides a fundamental spatial distribution for reservoir and geomechanics properties. In addition, this model will make an opportunity to generate a hydromechanical coupled dynamic numerical model which is a prior tool for analyzing various scenarios e.g., drilling, injection, production, etc. by considering the geomechanics effects in the future.

The structure of the manuscript is disposed of as follows. Firstly, the 1D geomechanical modeling is calculated at well locations by using log data. Secondly, the 1D reservoir modeling is computed at well locations by using well log data. Thirdly, the 3D geomechanical properties are distributed using geostatistical methods. Fourthly, the 3D reservoir properties are presented using geostatistical algorithms. Fifthly, the 3D static reservoir geomechanical modeling is built comprised of the 3D geomechanical and reservoir modeling which provides an opportunity for future dynamic scenarios. Finally, a summary and conclusions are provided.

Case study: Volve oil field, Norway

Description of the study area

This study is done based on the data from the Volve oil field, located in the central part of the North Sea, as shown in Fig. 1. The stratigraphic chart of the Volve oil field is given in Table 1. This oil field was discovered in 1993, and the plan for development was approved in 2005 (Sen and Ganguli 2019). Field production was launched in early 2008, achieving 56,000 bbl/day of peak oil rate. The main drainage strategy was pressure maintenance by water injection, with production wells placed high on the structure and water injectors at the flanks. The Volve field is described as a fault block structure with an initial estimate of 173 million bbl of oil in place (Equinor 2021). The reservoir is a small dome-shaped structure and is believed to be formed due to the collapse of adjacent salt ridges during the Middle Jurassic age (Equinor 2021; Szydlik et al. 2006). Oil was produced from the sandstone of the Middle Jurassic age in the Hugin formation at an average depth of $2700 \, to \, 3100m$ true vertical depth (TVD) below sea level. The recovery rate of Volve field was about 54% and it was shut down in 2016 after eight years of field operation.

Equinor company together with other operators of Volve filed have released all datasets. Released data consist of subsurface geology, geophysics, borehole logs, and various

Fig. 1 The geographic location of the Volve field (Wang et al. 2021)

Table 1 The stratigraphic chart of the Volve oil field (Sen and Ganguli, 2019)

System	Group	Formation	Lithology
Quaternary	Nordland	Recent sediments	Sandstone, Claystone
		Upper Utsira Formation	Sandstone
Tertiary	Hordaland	Lower Utsira Formation	Claystone
		Skade Formation	Sandstone, Claystone
		Grid Formation	Sandstone, Claystone
	Rogaland	Balder Formation	Claystone, Anhydride
		Sele Formation	Claystone
		Lista Formation	Claystone
		Ty Formation	Sandstone, Claystone,minor,Limestone
Cretaceous	Shetland	Ekofisk Formation	Limestone
		Tor Formation	Limestone
		Hod Formation	Limestone
		Blodoeks Formation	Limestone
		Hidra Formation	Limestone
	Cromer Knoll	Roedby Formation	Marl
		Asgard Formation	Marl, Limestone
Jurassic	Viking	Draupne Formation	Claystone, minor Limestone
		Heather Formation	Claystone
	Vestland	Hugin Formation	Sandstone, minor, Claystone and Limestone
		Sleipner Formation	Sandstone, Claystone intercalation, minor Coal

drilling and production reports (Equinor 2021). For this study, nine wells are selected that are included F-1A, F-1B, F-4, F-5, F-11T2, F-14, F-15A, F-15B, and F-15C.

Geological setting

The petrophysical and geomechanical information applied in this study is related to nine wells in the Volve oil field. The reservoir part of this field is related to Hugin and Heather formations and the caprock of this field is related to the Draupne formation. This field is composed of formations (zones) such as Hordaland, Grid, Balder, Sele, Lista, Ty, Ekofisk, Tor, Hod, Blodoks, Hidra, Rodby, Asgard, Draupne, Heather, Hugin, Sleipner, Mime, Skade, Skagerrak, Utsira, Smith Bank, Tryggvason, and Heimdal. Geological and petrophysical studies show that the rocks of the field for each formation are mainly sandstone, limestone, siltstone, claystone, calcite, marl, tuff, and coal as the lithology of each formation is shown in Fig. 2. The Volve oil field is geologically complex and requires precise knowledge of geology, tectonic structures, geophysical-seismic, and petrophysical section. One of these complexities can be mentioned in faults in the field (3D shape of the reservoir is shown in Fig. 3). Therefore, accurate estimation of petrophysical and geomechanical parameters with this volume of anisotropy is a very complex task and requires appropriate experimental knowledge in the field of geology, petrophysics, and geomechanics.

Methodology

In this study, all available data in the Volve oil field are collected, including geological, geophysical, petrophysical, and geomechanical data. The workflow adopted for the static reservoir geomechanical model is indicated in Fig. 4. The structural interpretation of this study is performed using seismic data. The workflow starts with 1D modeling of each well to determine petrophysical and geomechanical properties. 1D petrophysical parameters are evaluated using well log data from nine wells. 1D geomechanical properties are calculated using well log data from nine wells. The main focus of this article is on petrophysical and geomechanical modeling for porosity, permeability, hydrocarbon saturation, pore pressure, elastic properties, vertical stress, and horizontal stresses. Core data have been used to evaluate the accuracy of petrophysical and geomechanical well data.

Static modeling consists of two main parts. The first part of structural modeling is the process of making a skeleton or a 3D reservoir geomechanical network (Avseth et al. 2005; Cannon 2018). The second part is petrophysical and geomechanical data analysis and static reservoir geomechanical modeling. The process of petrophysical and geomechanical data analysis consists of (1) upscaling the well log, (2) analyzing the data, (3) geocell modeling, and (4) petrophysical modeling. The 3D reservoir geomechanical model is built based on a structural/geological model which is generally done by using data of seismic and borehole information. Previous studies expressed that the upscaling
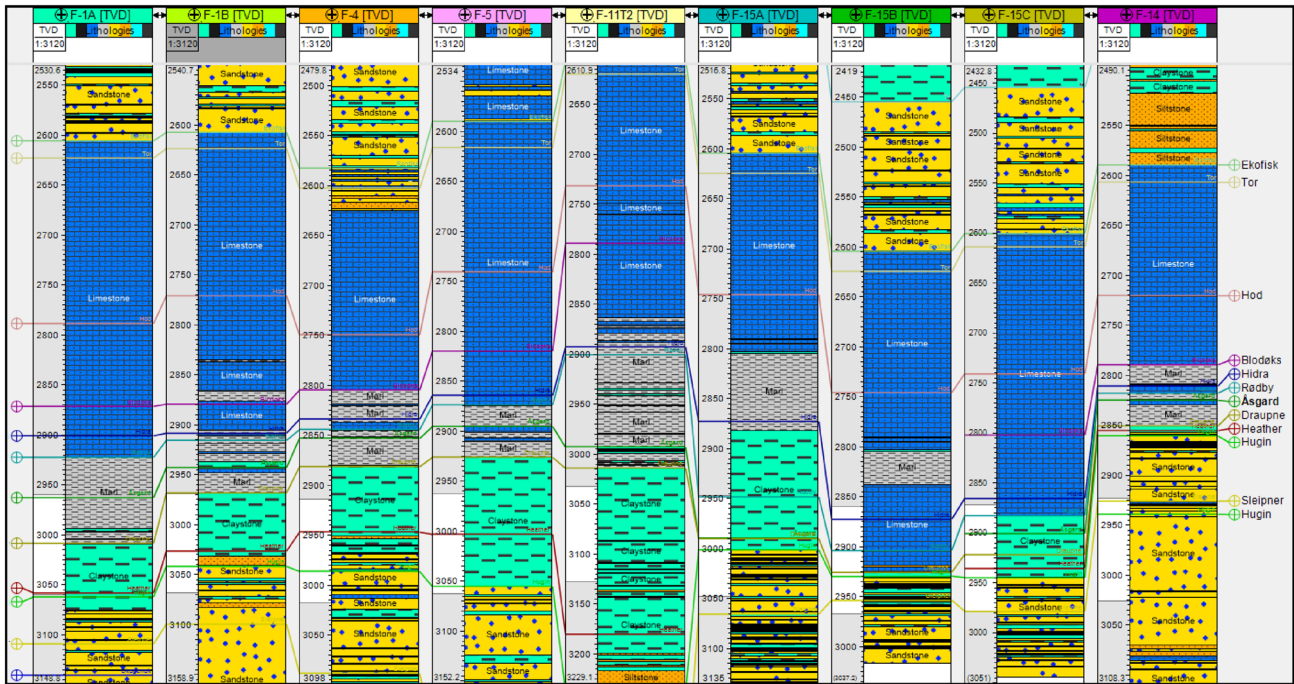
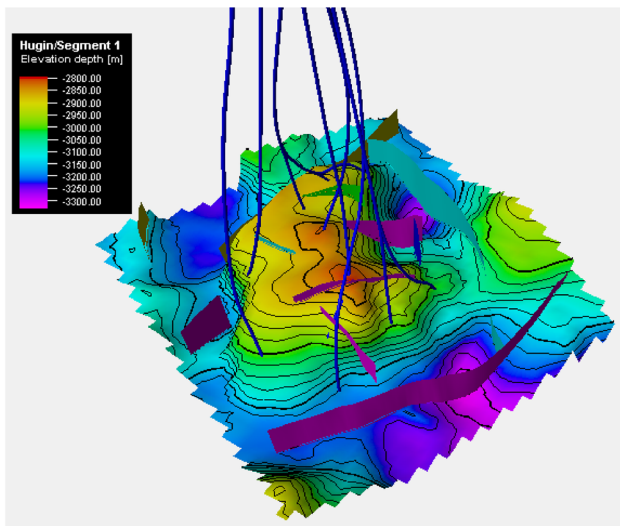**Fig. 2** Stratigraphic column of the studied formations in the Volve oil field, Norway

Fig. 3 Three-dimensional shape of Volve oil field, Norway

of geomechanical and petrophysical properties from various 1D models to the 3D models can be done successfully through geostatistical methods such as Gaussian and Kriging interpolation schemes (Kim et al. 2002; Amanipoor et al. 2019; Adewunmi et al. 2019; Zain et al. 2020). Then, the upscaling of geomechanical properties such as pore pressure, horizontal stresses, vertical stresses, Young modulus, Poisson ratio, and unconfined compressive strength (UCS) from 1D models to 3D models are done using the geostatistical

methods. Moreover, the upscaling of reservoir characterizations such as porosity, permeability, and hydrocarbon saturation are done from 1D models to 3D models using geostatistical methods.

The 3D static reservoir geomechanical model which is composed of the combination of the reservoir and geomechanical model can be used to make a coupled geomechanics and fluid flow model (dynamic reservoir). Generally, Geomechanics and dynamic reservoir model are coupled iteratively through pore pressure and effective stresses that cause rock deformation, which affects the porosity and permeability of the reservoir. Then, the coupled dynamic reservoir geomechanics can be applied to future studies, such as production, injection, and history matching. The workflow adopted for the future dynamics reservoir geomechanical scenarios is shown in Fig. 5.

The 1D reservoir geomechanics modeling

The one-dimensional 1D modeling of reservoir geomechanics comprises the 1D geomechanical modeling and the 1D petrophysical (reservoir) properties modeling that are presented as follows:

The 1D geomechanical modeling

1D geomechanical modeling is a continuous numerical representation of geomechanical properties, pore pressure, and
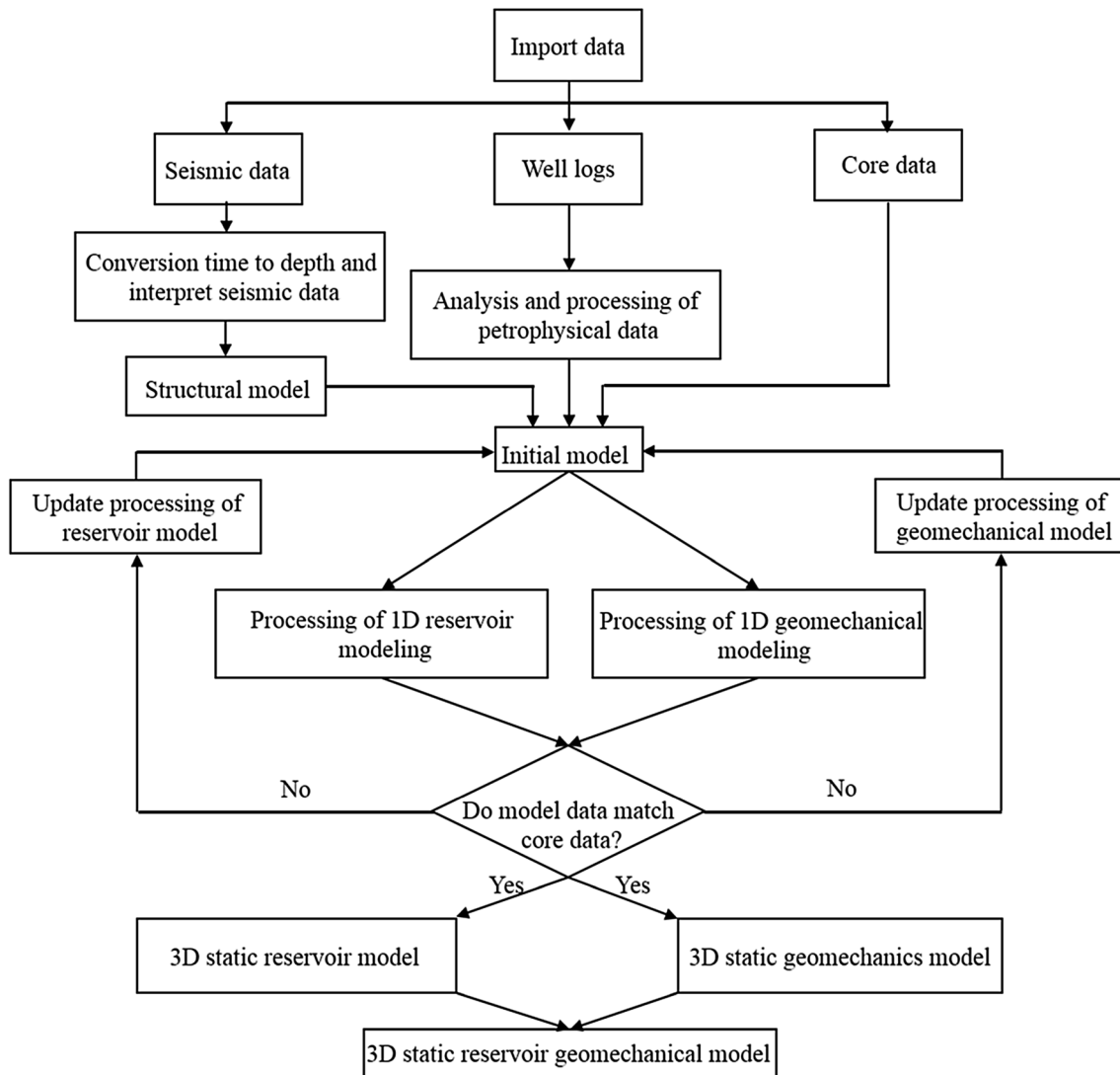
Fig. 4 Flowchart adopted for the static reservoir geomechanical model

the in situ stresses along a borehole (Plumb et al. 2000). To represent the geomechanical modeling, well log data are used to estimate various material properties, pore pressure, and in situ stresses along a wellbore. The quality of a 1D geomechanical model depends on the quality and availability of well log data and laboratory test data.

Estimation of vertical stress

Vertical stress is the pressure applied by the overlaying lithostatic column, at the depth (z), and can be estimated by the following equation (Plumb et al. 1991):

$$S_v = \int_0^z \rho(z)\, g\, dz \qquad (1)$$

where, S_v is the vertical stress, $\rho(z)$ is the bulk density, and g is the gravitational acceleration.

The vertical stress is estimated from density logs and the results for well F1A are shown in Fig. 6.

Estimation of minimum horizontal stress

Minimum horizontal stress can be estimated from well-log data using different empirical equations such as Eaton (1968), Blanton and Olson (1999), poroelastic equations (Fjar et al. 2008), etc. In this study, the minimum horizontal stress S_h is calculated using the Blanton's relationship (Blanton and Olson 1999), as follows:

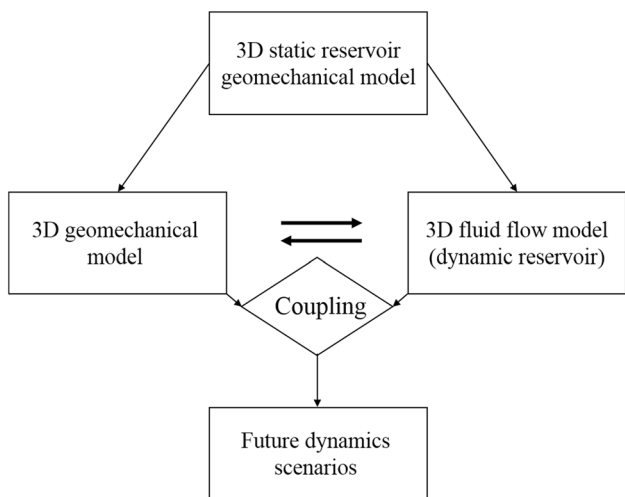$$S_h = k * \left(S_v - p_p\right) + p_p + S_{tec} \qquad (2)$$

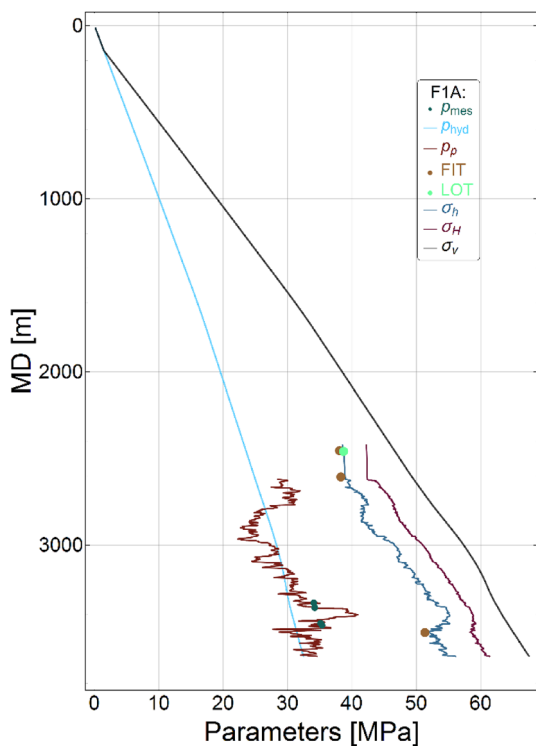**Fig. 5** Flowchart adopted for the future dynamics reservoir geomechanical scenarios

Fig. 6 The graph includes a comparison of measured pore pressure p_{mes} with the results of the Eaton model p_p, a comparison of measured minimum horizontal stress *FITandLOT* with the results of the Blanton model σ_h, hydrostatic pressure p_{hyd}, maximum horizontal stress σ_H, and vertical stress σ_V for well F1A

where S_v is the vertical stress, p_p is the pore pressure, and k is the coefficient of the earth's stress. The tectonic stress S_{tec} is represented as (Daines 1982):

$$S_{tec} = F - \left[(S_v - p_p) * \left(\frac{\nu}{1-\nu} \right) + p_p \right] \tag{3}$$

where F is the fracture reopening and ν is the Poisson's ratio.

The minimum horizontal stress is estimated from sonic logs using Blanton's equation The results of the well F1A show that the Blanton model can estimate minimum horizontal stress accurately as illustrated in Fig. 6.

Maximum horizontal stress

To calculate the maximum horizontal stress, the poroelastic theory can be used. The poroelastic relationships are presented as follows (Blanton and Olson 1999):

$$S_H = \frac{\nu}{1-\nu}\sigma_v - \frac{\nu}{1-\nu}\alpha p_p + \alpha p_p + \frac{E}{1-\nu^2}\varepsilon_x + \frac{\nu E}{1-\nu^2}\varepsilon_y \tag{4}$$

where E is the Young modulus, ν is the Poisson's ratio, α is the Biot's coefficient, ε_x and ε_y are the strain in the x and y direction, respectively.

The maximum horizontal stress is estimated from poroelastic theory and the results for well F1A are shown in Fig. 6.

Estimation of pore pressure

Pore pressure can be estimated from well log data using different empirical equations such as Eaton (1975), Gardner et al. (1974), Bowers (1995), etc. In this study, pore pressure is estimated from resistivity and sonic logs using the well-known Eaton's equation (Eaton 1975). The equation of Eaton is:

$$p_p = S_v - (S_v - p_{hyd}) \times \left(\frac{DT_n}{DT} \right)^a \tag{5}$$

where S_v is the overburden stress and DT is the measured sonic transit time available from compressional sonic well logs. The DT_n is the sonic transit time on the normal line which can be estimated using Zhang's equation (Zhang 2011), as follows:

$$DT_n = DT_{sh} + (DT_{ml} - DT_{sh})e^{-cz} \tag{6}$$

where DT_{sh} is the compressional transit time in the shale matrix, DT_{ml} is the mudline transit time, c is the constant, and z is the depth. The hydrostatic pressure p_{hyd} is:

$$p_{hyd} = \int_0^z \rho_w(z)\, g\, dz \tag{7}$$

where ρ_w is the density of water. In this study, the average gradient of hydrostatic pressure is 1.03 g/cm³.
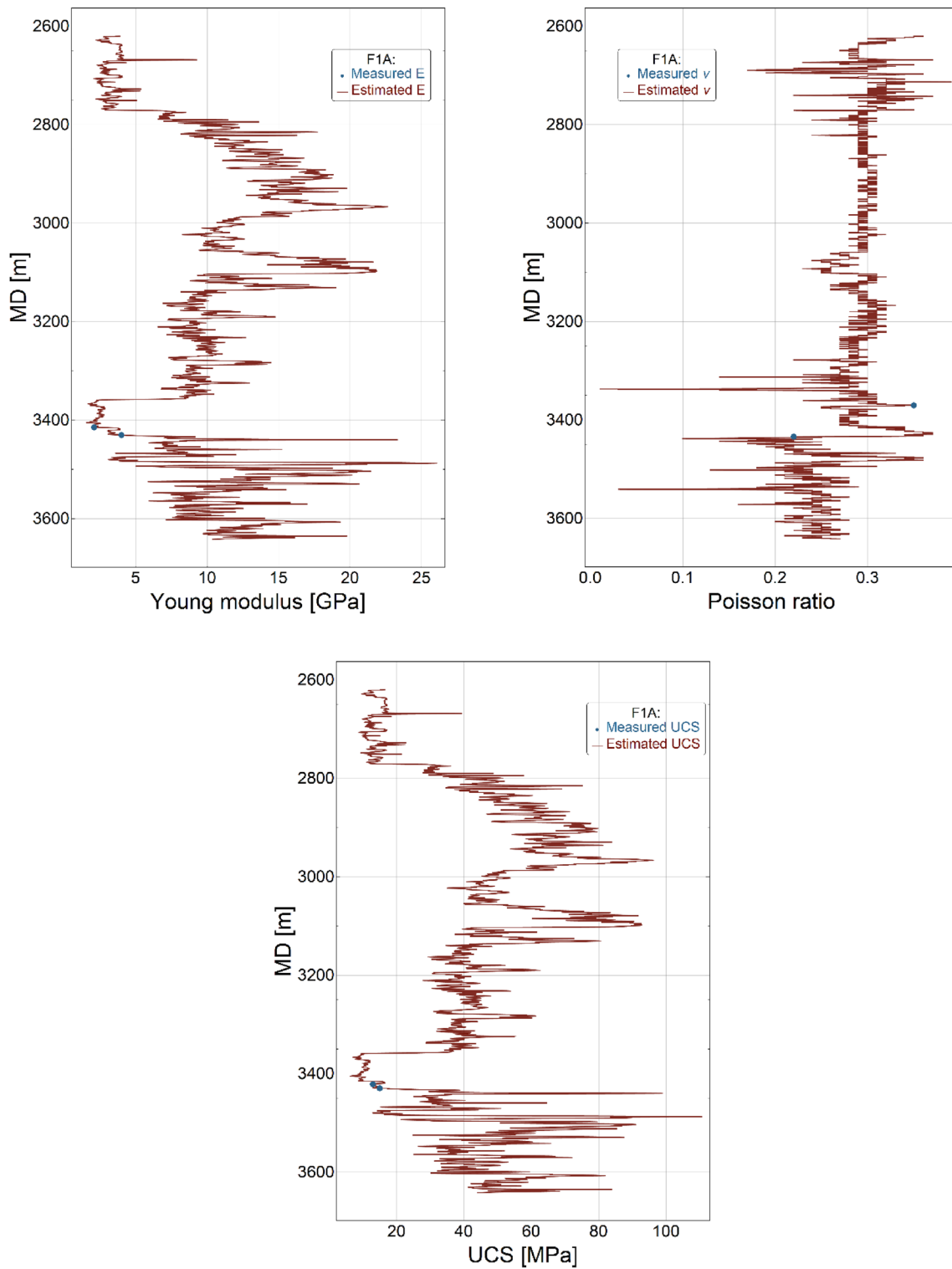
Fig. 7 The comparison of measured (top-left) static Young modulus *E* with the results of John Fuller model, (top-right) Poisson ratio *ν* with the results of the position ratio with the multiplier, ml = 1, and (bottom) unconfined compressive strength *UCS* with the results of the Dick Plumb model for well F1A
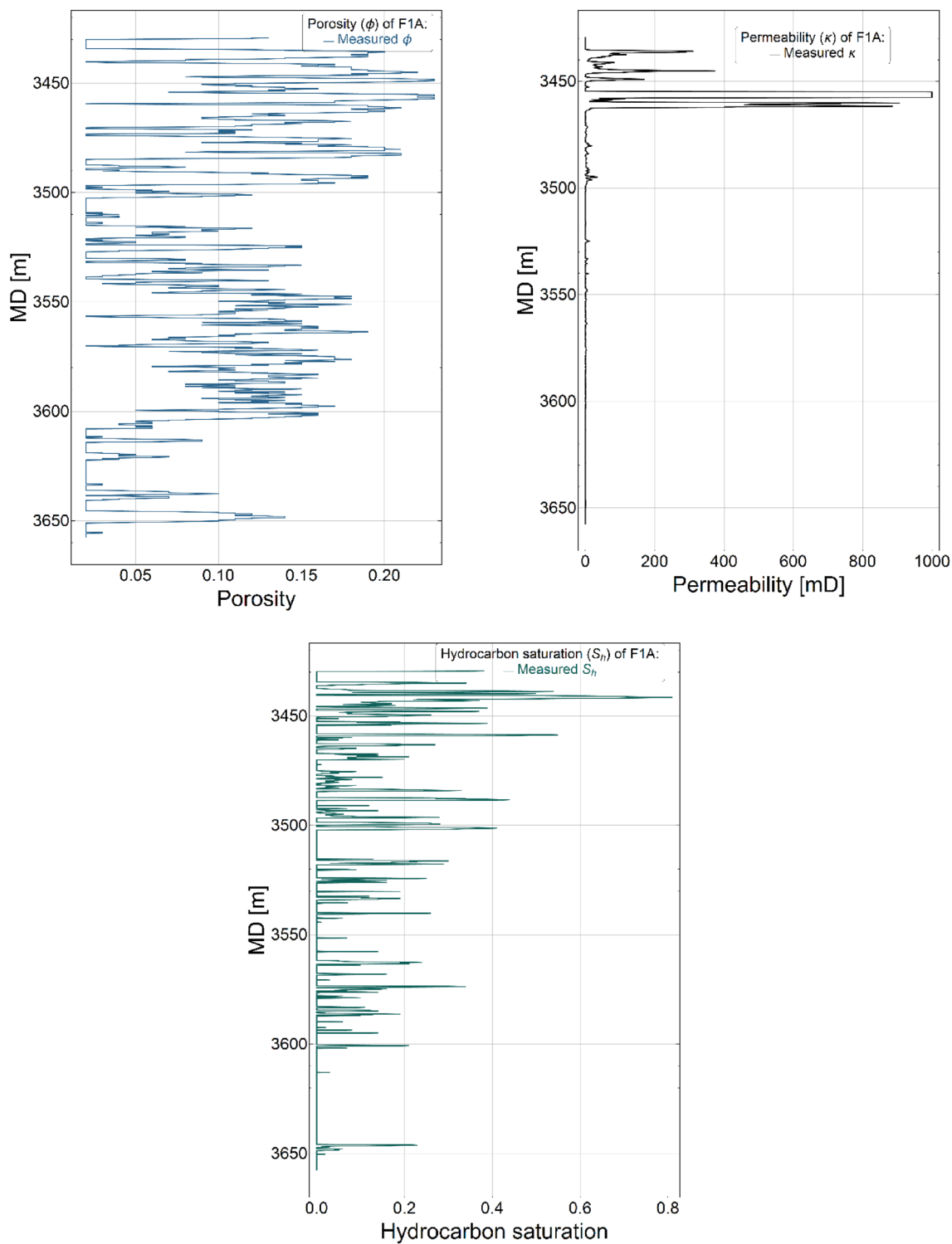
Fig. 8 The graph includes: (top- left) porosity ϕ, (top-right) permeability k, and (bottom) hydrocarbon saturation S_h

The pore pressure is estimated from sonic logs using Eaton's equation The results for well F1A indicate that the Eaton model can estimate pore pressure precisely as shown in Fig. 6.

In Fig. 6, laboratory core data are used to evaluate the accuracy of geomechanical properties. It shows a good agreement between measured and numerical results of pore pressure and minimum horizontal stress. The same

Fig. 9 Static pore pressure distribution through upscaled computed 1D well log properties: (top) Kriging (Krig) method and (bottom) SGS method
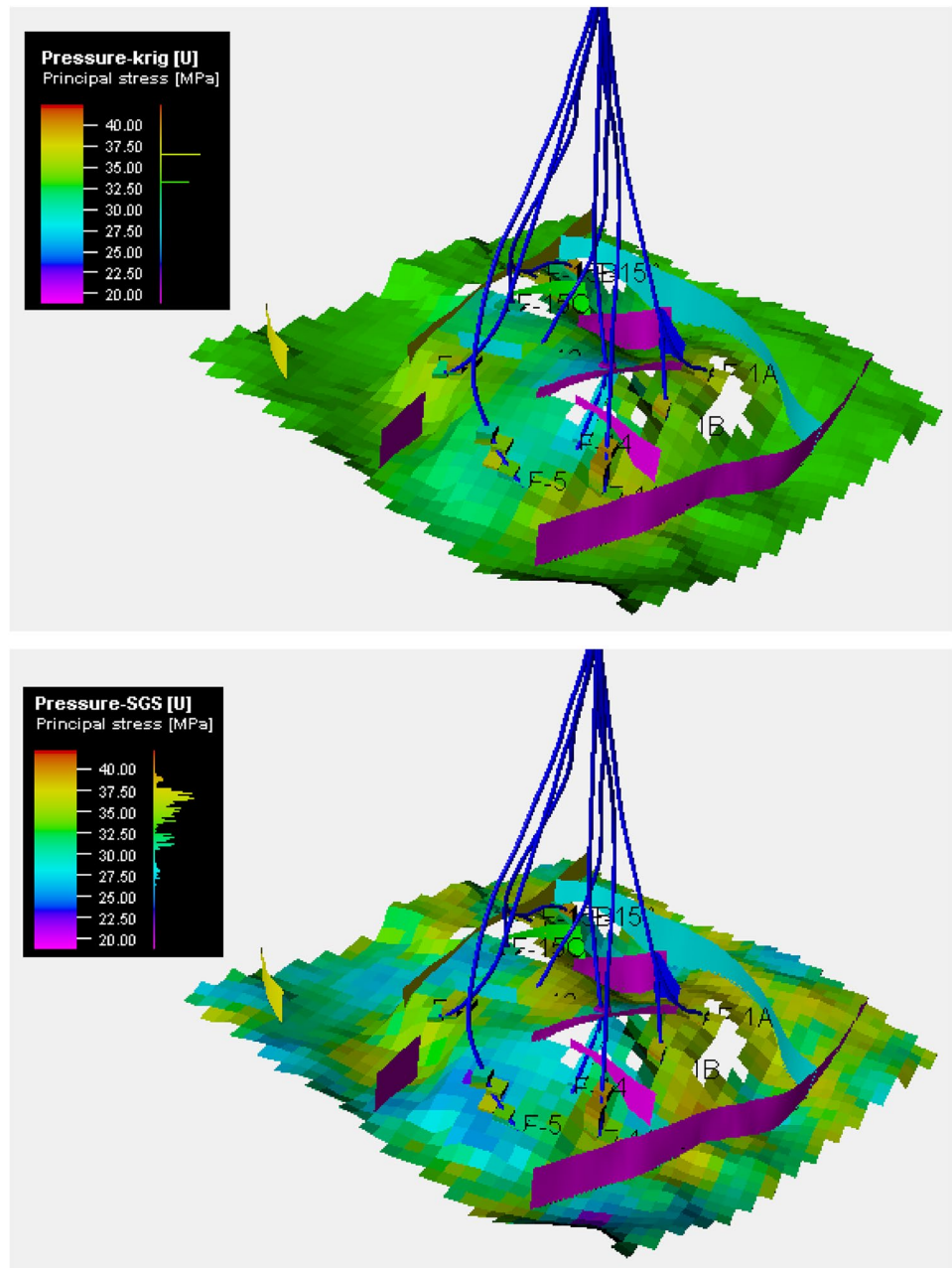
procedure described for building the 1D model of pore pressure, minimum horizontal stress, maximum horizontal stress, and vertical stress for well F1A as presented in Fig. 6 is performed for other wells.
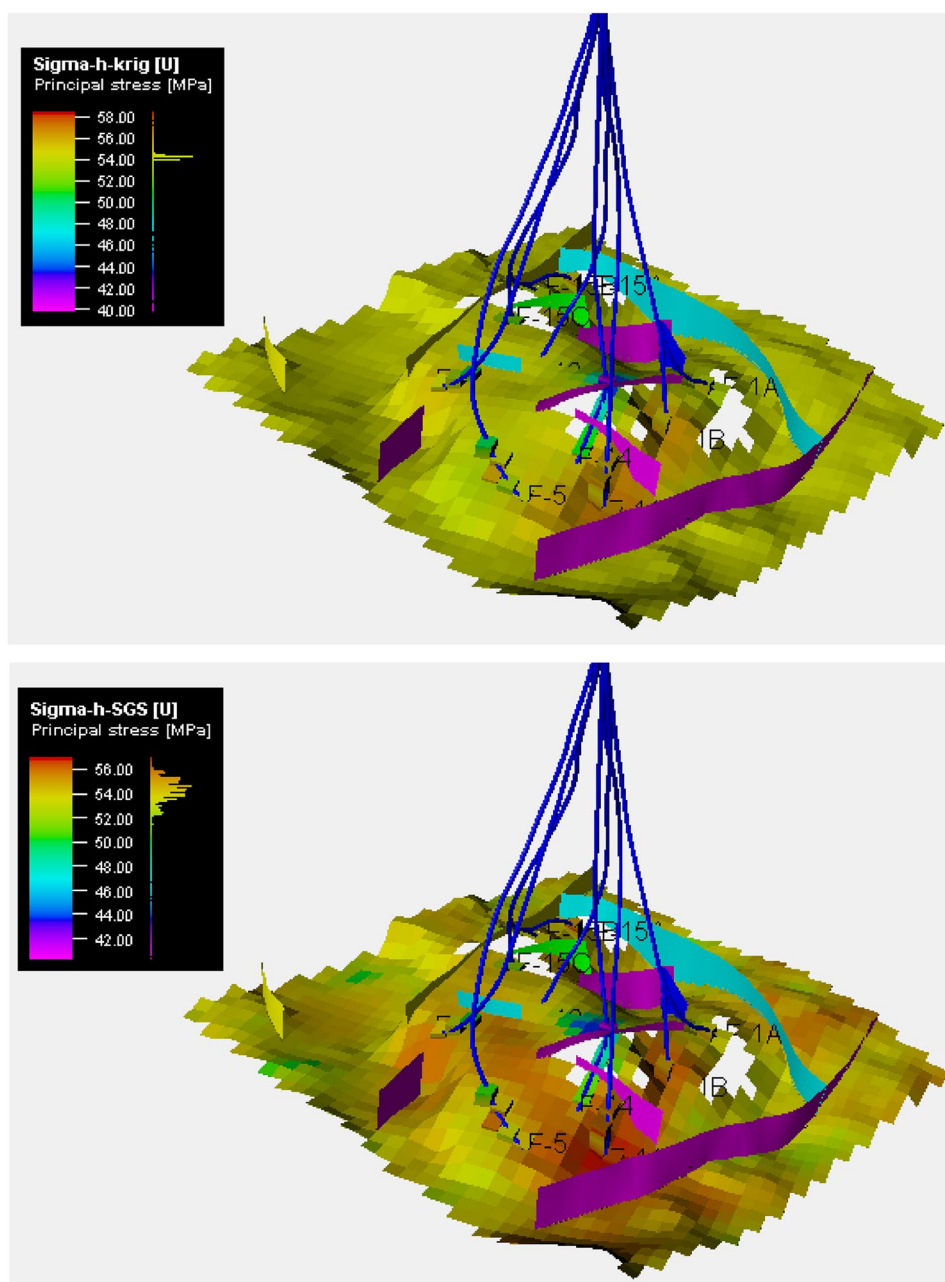
Elastic properties

The elastic parameters of the rock can be obtained using the density logs and sonic wave velocity (dynamic method). Given the assumption of a homogeneous and isotropic formation, the dynamic Young modulus $E_d [Gpa]$ and dynamic Poisson ratio $\nu_d [\%]$ are computed as (Fjær et al. 2008):

$$E_d = \rho V_s^2 \frac{3V_p^2 - 4V_s^2}{V_p^2 - V_s^2} \tag{8}$$

$$\nu_d = \frac{V_p^2 - 2V_s^2}{2\left(V_p^2 - V_s^2\right)} \tag{9}$$

where ρ is the bulk density of the formation [g/cm³], V_p is the compressional wave velocity [km/s], and V_s is the shear wave velocity [km/s].

Fig. 10 Static minimum horizontal stress distribution through upscaled computed 1D well log properties: (top) Kriging (Krig) method and (bottom) SGS method

Static elastic properties

To estimate the static parameters from dynamic parameters, several relationships have been proposed. In this study, the static Young modulus E_s [Gpa] is estimated using the John Fuller model (Schlumberger 2018) as expressed by the following equation:

$$E_s = 0.032 \times \left(E_d\right)^{1.632} \tag{10}$$

The static Young modulus is estimated from sonic logs using the John Fuller model. The results to well F1A show

that the John Fuller model can estimate the static Young modulus accurately as illustrated in Fig. 7.

The static Poisson ratio ν_s is computed from the dynamic Poisson ratio ν_d by the following relationship:

$$\nu_s = ml \times \nu_d \tag{11}$$

where ml is the multiplier. Some researchers, including Archer and Rasouli (2012) expressed that the ml = 1 means the static Poisson ratio is equal to the dynamic Poisson ratio. However, Afsari et al. (2009) presented that the ml = 0.7. In this study, the results for estimating the static Poisson ratio show that the best multiplier is ml = 1, as presented in Fig. 7.

Fig. 11 Static Young modulus distribution through upscaled computed 1D well log properties: (top) Kriging (Krig) method and (bottom) SGS method
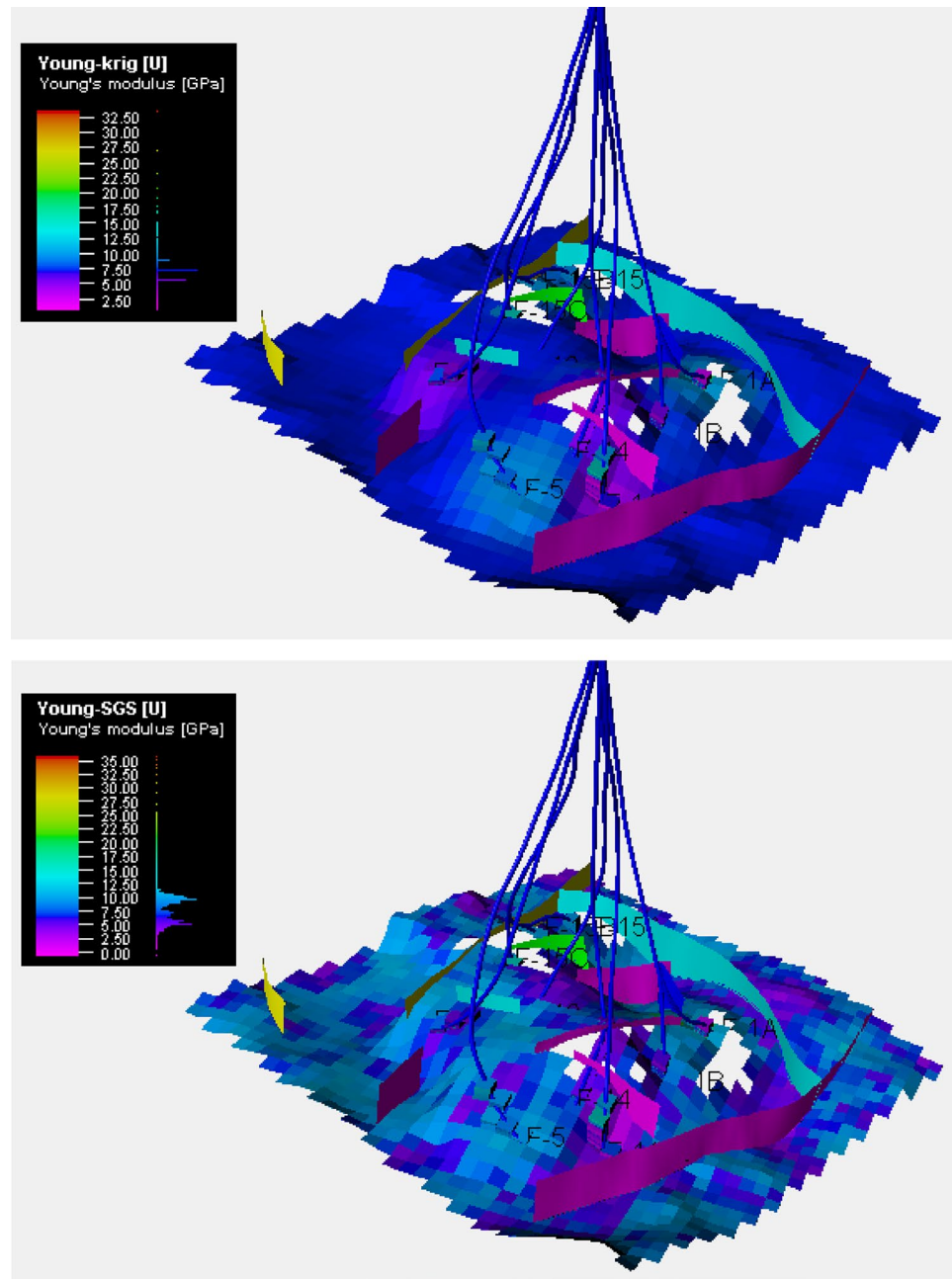
Unconfined compressive strength

The unconfined compressive strength (UCS) can be obtained using compressional wave velocity, density, and porosity logs. In this study, the unconfined compressive strength UCS [Gpa] is estimated using the Dick Plumb model (Schlumberger 2018) as expressed by the following equation:

$$UCS = 4.242 \times E_s \tag{12}$$

The unconfined compressive strength is estimated from the static Young modulus using the Dick Plumb model. The results to well F1A show that the Dick Plumb model can estimate the unconfined compressive strength accurately as shown in Fig. 7.

In Fig. 7, laboratory core data are used to evaluate the accuracy of geomechanical properties. It shows a good agreement between measured and numerical results of Young modulus, Poisson ratio, and unconfined compressive strength. The same procedure described for building the 1D model of static Young modulus, Poisson ratio, and UCS for well F1A as shown in Fig. 7 is performed for other wells.

Fig. 12 Static porosity distribution through upscaled computed 1D well log properties: (top) Kriging (Krig) method and (bottom) SGS method
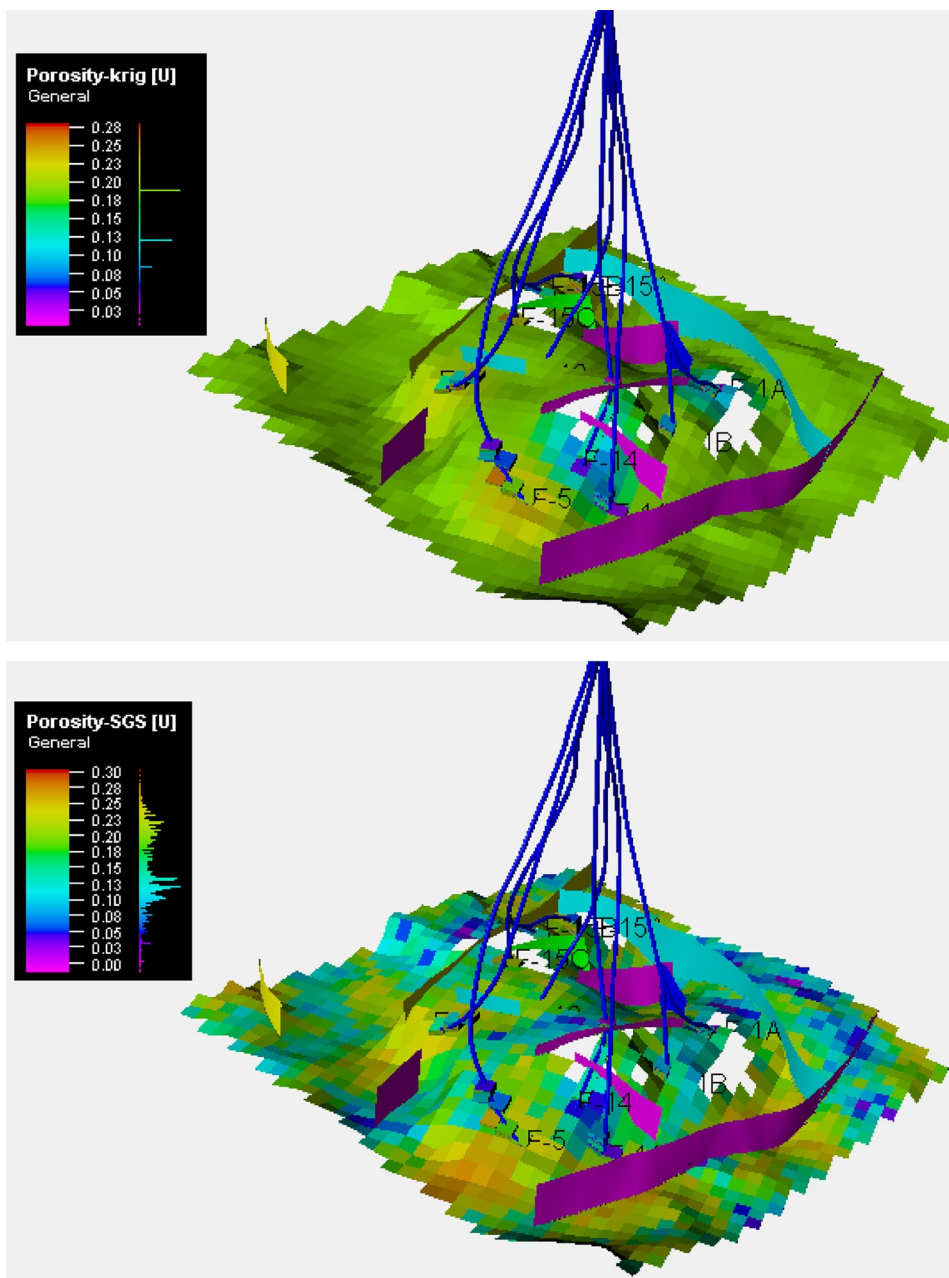
The 1D reservoir properties modeling

Well-log data are used to calculate reservoir (petrophysical) properties such as porosity, permeability, and hydrocarbon saturation. The 1D reservoir properties were computed and verified by Equinor (Equinor 2021) and in this study, the same procedure is done in order to be able to build the 3D static reservoir modeling. The process that the Equinor was done to make 1D reservoir properties are as follows:

Porosity

Total porosity ϕ is derived from the density log which is calibrated to overburden corrected core porosity (Tiab and Donaldson 2015). The Neutron log, NPHI, has been used to correct for varying mud filtrate invasion.

$$\phi = \phi_D + A \times \left(\text{NPHI} - \phi_D \right) + B \tag{13}$$

where

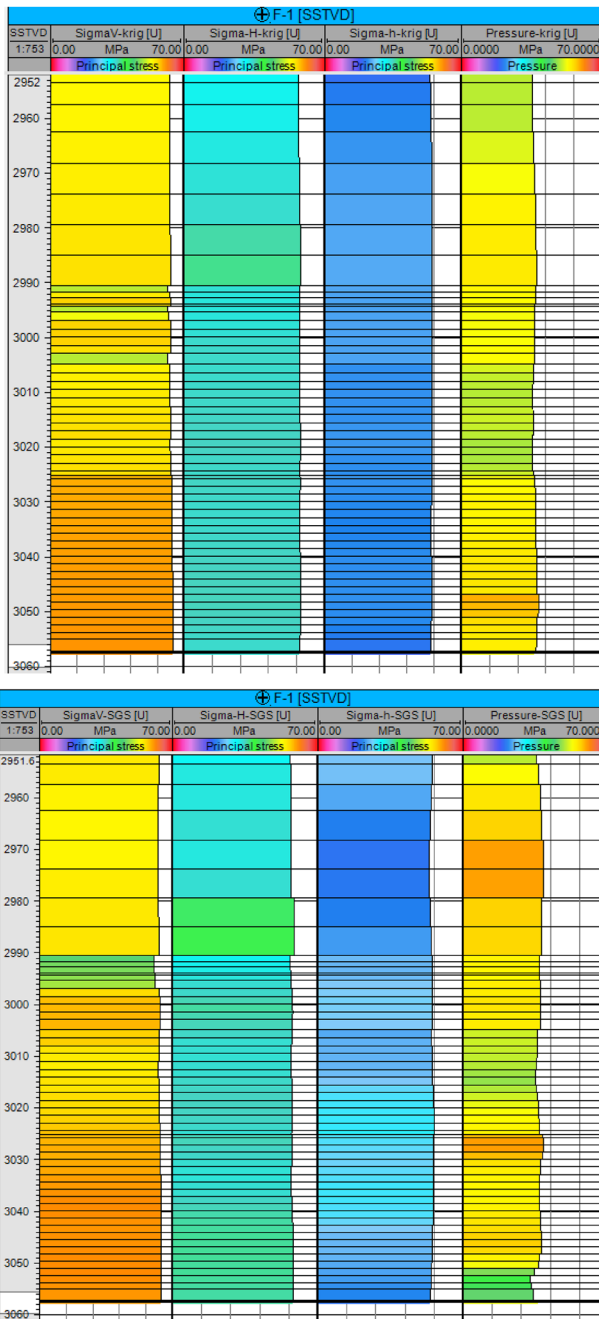$$\phi_D = \frac{\rho_{ma} - \rho_b}{\rho_{ma} - \rho_{fl}} \tag{14}$$

Fig. 13 The comprehensive prognosis of vertical stress, maximum horizontal stress, minimum horizontal stress, and pore pressure for a new position well, namely F1: (up) Kriging, and (bottom) SGS method

where ρ_{ma} is the matrix density [g/cm^3], ρ_b is the measured bulk density (RHOB) [g/cm^3], ρ_{fl} is the pore fluid density [g/cm^3], and A and B are regression coefficients.

The porosity for well F1A is obtained from Eq. 13 and the results are illustrated in Fig. 8.

Permeability

The permeability k is derived from the following equation based on multivariable regression analysis between log porosity and shale volume against overburden corrected core permeability.

$$k = 10^{(2+8*\phi-9\times VSH)} \tag{15}$$

where VSH is the shale volume.

The permeability for well F1A is obtained from Eq. 15 and the results are indicated in Fig. 8.

Hydrocarbon saturation

Hydrocarbon saturation can be calculated from water saturation. The water saturation S_w is obtained using Archie equation (Tiab and Donaldson 2015) as follows:

$$S_w = \left(\frac{a \times R_w}{\phi^m * R_t} \right)^{\frac{1}{n}} \tag{16}$$

where a is the Archie factor, R_w is the resistivity of formation water [$ohmm$], m is the cementation exponent, R_t is the true resistivity [$ohmm$], and n is the saturation exponent.

The hydrocarbon saturation S_h can be obtained as follows (Tiab and Donaldson 2015):

$$S_h = 1 - S_w \tag{17}$$

The hydrocarbon saturation for well F1A is obtained from Eq. 17 and the results are shown in Fig. 8.

The same procedure described for building the 1D model of porosity, permeability, and hydrocarbon saturation for well F1A as illustrated in Fig. 8 is performed for other wells.

The 3D model generation

The three-dimensional modeling of reservoir geomechanics comprises the 3D geomechanical model and 3D static reservoir model. Each model comprises the reservoir geology, structure, stratigraphic, reservoir sublayers, and faults in 3D structural and properties models.

The 3D geomechanical model

The 3D static geomechanical model is built up using the structural/geological model with high resolution. The 3D geomechanical properties are distributed by geostatistical methods based on the 1D geomechanical models from the log data. The geostatistical methods such as the Kriging and Gaussian (Sequential Gaussian Simulation (SGS)) method are used to populate the 3D geomechanical model.

The 3D reservoir model

The 3D static reservoir model is built up using the structural/geological model with a high resolution. The reservoir volume is divided into a 3D mesh of cells and for each cell, rock properties are assigned. The 3D reservoir properties are distributed using the upscaled 1D (reservoir) petrophysical models from the log data. The geostatistical methods such as the Kriging and Gaussian (Sequential Gaussian Simulation (SGS)) method are used to populate the 3D reservoir model.

Results

The 3D geomechanical properties modeling

The geomechanical properties such as pore pressure, horizontal stresses, vertical stress, Young's modulus, Poisson's ratio, and unconfined compressive strength are upscaled and populated by the Kriging and Gaussian (Sequential Gaussian Simulation (SGS)) methods. The geomechanical properties show distinct vertical variations, but only slight lateral changes because of changes in lithology. The spatial distribution of each property is obtained using the upscaled methods and the results of them are presented as follows:

The spatial distribution of pore pressure using both Kriging and SGS methods are presented in Fig. 9. The pore pressure ranges from 19.46 Mpa to 41.62 MPa. The average value of the pore pressure is 33.63 MPa.

The spatial distribution of minimum horizontal stress using both Kriging and SGS methods is presented in Fig. 10. The minimum horizontal stress ranges from 40.79 MPa to 57.03 MPa. The average value of the minimum horizontal stress is 53.23 MPa.

The spatial distribution of maximum horizontal stress using both Kriging and SGS methods is presented in Appendix A. The maximum horizontal stress ranges from 44.99 MPa to 61.79 MPa. The average value of the maximum horizontal stress is 56.49 MPa. Moreover, the spatial distribution of vertical stress using both Kriging and SGS methods is presented in Appendix A. The vertical stress ranges from 49.15 MPa to 66.54 MPa. The average value of the vertical stress is 60.51 MPa. In addition, the spatial distribution of the Young modulus using both Kriging and SGS methods is presented in Fig. 11. The Young modulus ranges from 0.55 GPa to 33.58 GPa. The average value of the Young modulus is 7.50 GPa.

The spatial distribution of the Poisson ratio using both Kriging and SGS methods is presented in Appendix A. The Poisson ratio ranges from 0.12 to 0.44. The average value of the Poisson ratio is 0.28. Furthermore, the spatial distribution of unconfined compressive strength UCS using both Kriging and SGS methods is presented in Appendix A. The UCS ranges from 2.34 MPa to 142.42 MPa. The average value of the UCS is 31.93 MPa.

The 3D reservoir properties modeling

The reservoir properties such as porosity, permeability, and hydrocarbon saturation are upscaled and populated by the Kriging and SGS methods. The spatial distribution of each property is obtained using the upscaled methods and the results of them are presented as follows:

The spatial distribution of porosity using both Kriging and SGS methods is presented in Fig. 12. The porosity ranges from 0 to 0.28. The average value of the porosity is 0.15.

The spatial distribution of permeability using both Kriging and SGS methods is presented in Appendix B. The permeability ranges from 0 mD to 34,148 mD. The average value of the permeability is 412.99 mD. Moreover, the spatial distribution of hydrocarbon saturation using both Kriging and SGS methods is presented in Appendix B. The hydrocarbon saturation ranges from 0 to 0.99. The average value of the hydrocarbon saturation is 0.38.

Discussions

Future dynamic scenarios

The 3D reservoir geomechanical model gives the opportunity to assess the drilling and production conditions (potential and risk) of a new well at any location within the domain of the reservoir. For instance, in the drilling operation, planning of a well trajectory requires information about the pore pressure and the full stress tensor, i.e., the magnitude and the orientations of all three principal stresses. This fundamental information is essential, especially near faults and other geological complexities. Such a comprehensive prognosis of pore pressure and stress tensor can be provided by the 3D reservoir geomechanical model, as in this section, the pore pressure and stress tensor for a new position well, namely F1 are shown in Fig. 13. This method of stress tensor prediction based on the 3D reservoir geomechanical model can be universally used.

Summary and Conclusions

A workflow of reservoir geomechanical numerical modeling has been proposed. It combines the 1D and 3D models of geomechanics and reservoir to construct the 3D static reservoir geomechanical model. The following remarks can be outcomes of this paper:

- A systematic procedure for the construction of a 1D geomechanical model is developed to calculate the pore pressure, horizontal stresses, vertical stress, Young modulus, Poisson ratio, and unconfined compressive strength. The numerical results of this procedure are in agreement with measured data.

- The same procedure as the 1D geomechanical model is presented to determine the reservoir characteristics such as porosity, permeability, and hydrocarbon saturation.
- The 3D reservoir and geomechanical properties are distributed by using geostatistical methods such as Kriging and Gaussian from the 1D reservoir and geomechanical model. The 3D static reservoir geomechanical model is composed of the combination of the 3D reservoir and geomechanical model. This 3D model is an effective tool for a better understanding of the spatial distribution of reservoirs and geomechanical properties.
- The 3D static reservoir geomechanical model provides the complete state of parameters such as pore pressure, in-situ stresses, elastic properties, and reservoir char-

acterization at any location in the model domain. This information as prior tools can be applied to the planning of future wells and reservoir scenarios.

Appendix

Appendix A Three-dimensional static geomechanical modeling

The spatial distribution of the maximum horizontal stress, vertical stress, Poisson ratio, and UCS by using both Kriging and SGS methods is presented in FigS. 14, 15, 16, and 17, respectively.

Fig. 14 Static maximum horizontal stress distribution through upscaled computed 1D well log properties: (top) Kriging (Krig) method and (bottom) SGS method
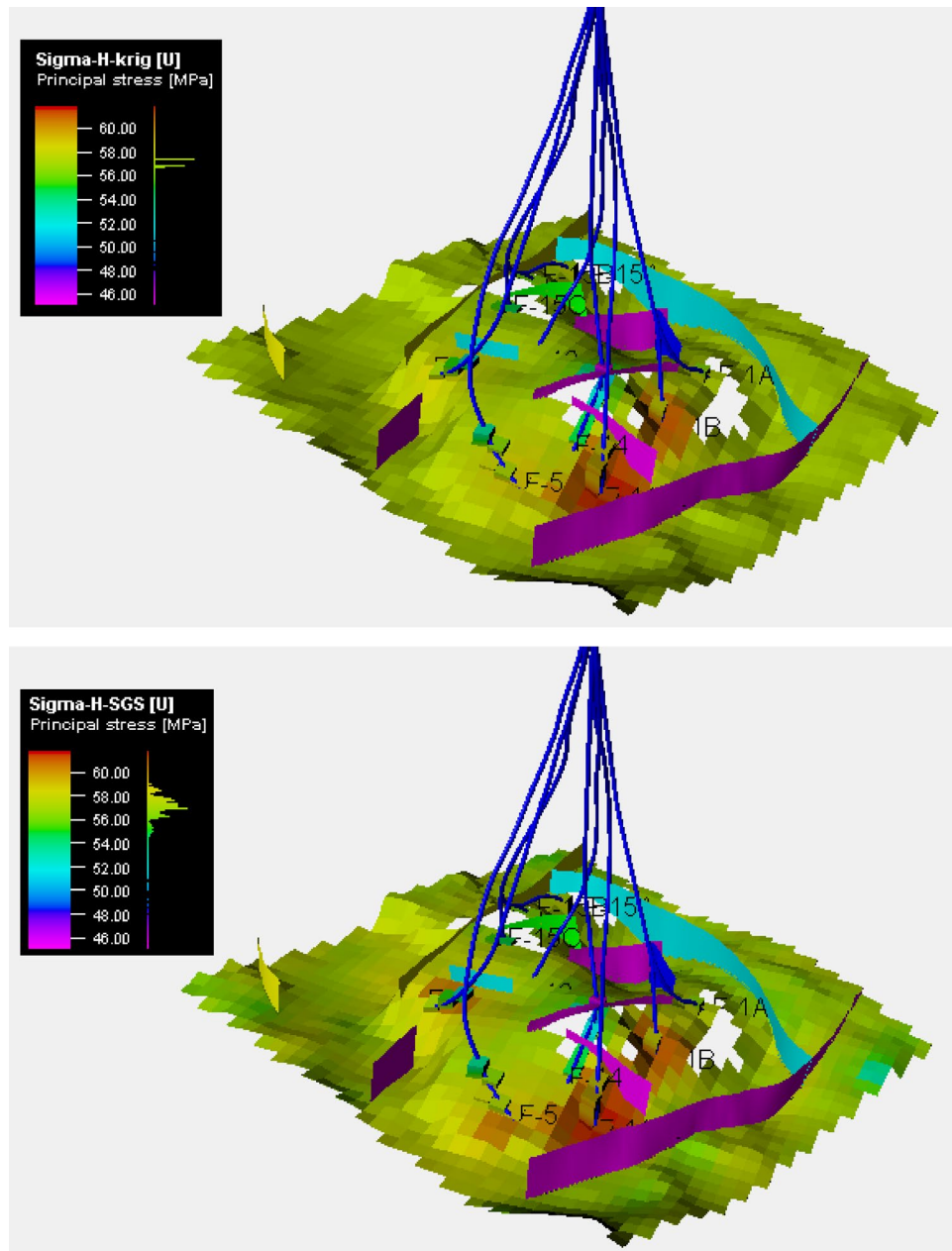
Fig. 15 Static vertical stress distribution through upscaled computed 1D well log properties: (top) Kriging (Krig) method and (bottom) SGS method
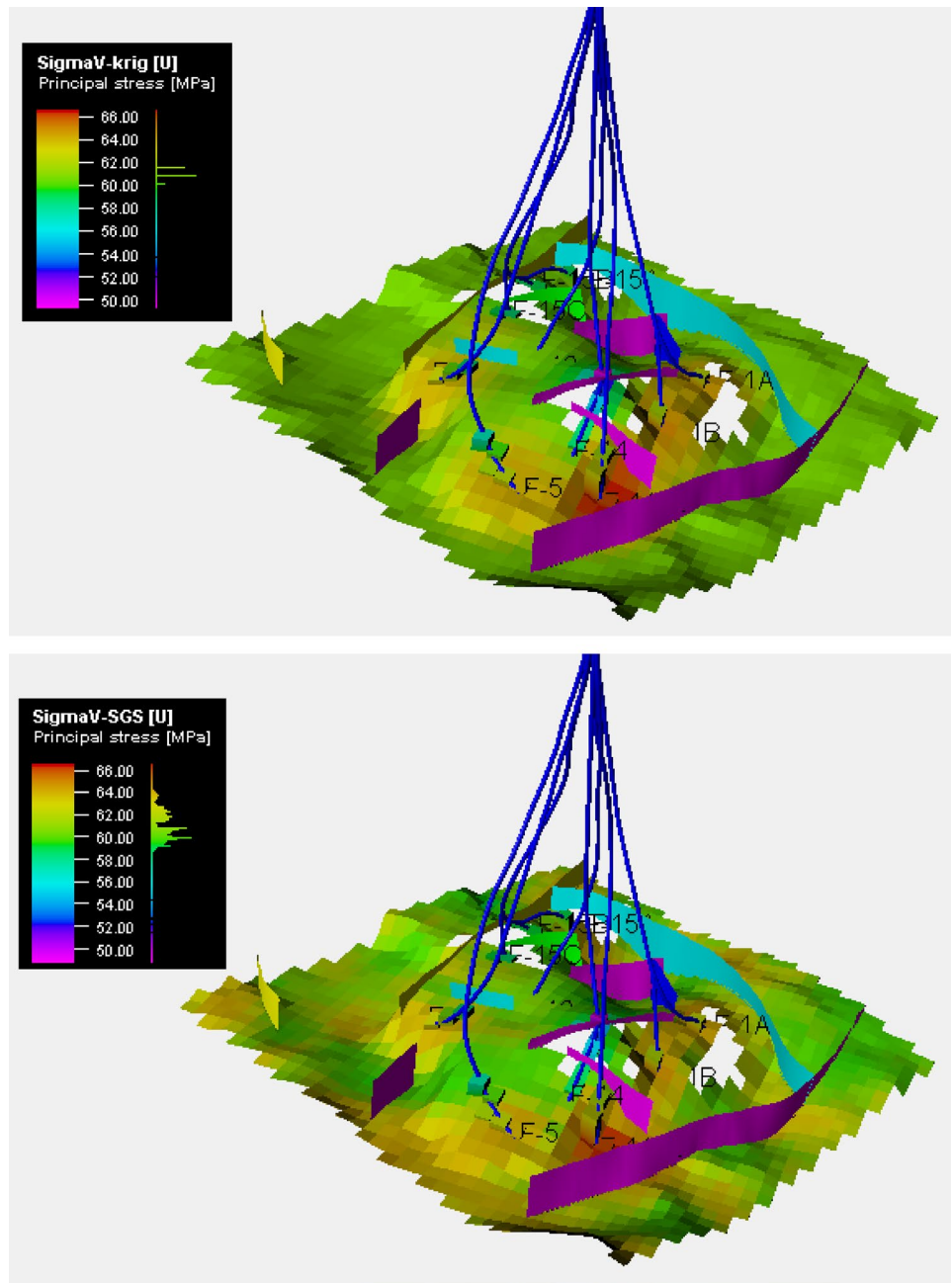
Fig. 16 Static Poisson ratio distribution through upscaled computed 1D well log properties: (top) Kriging (Krig) method and (bottom) SGS method
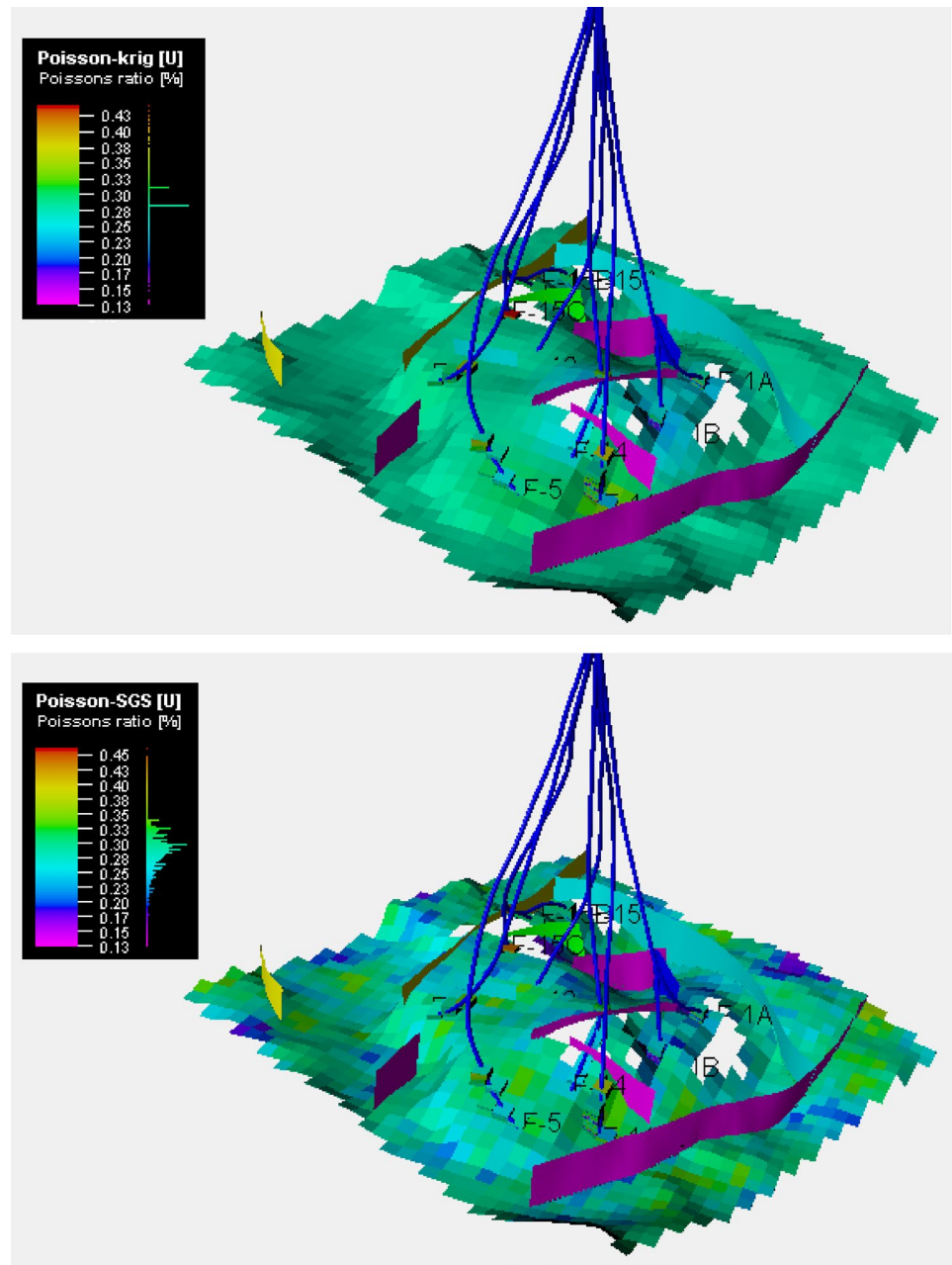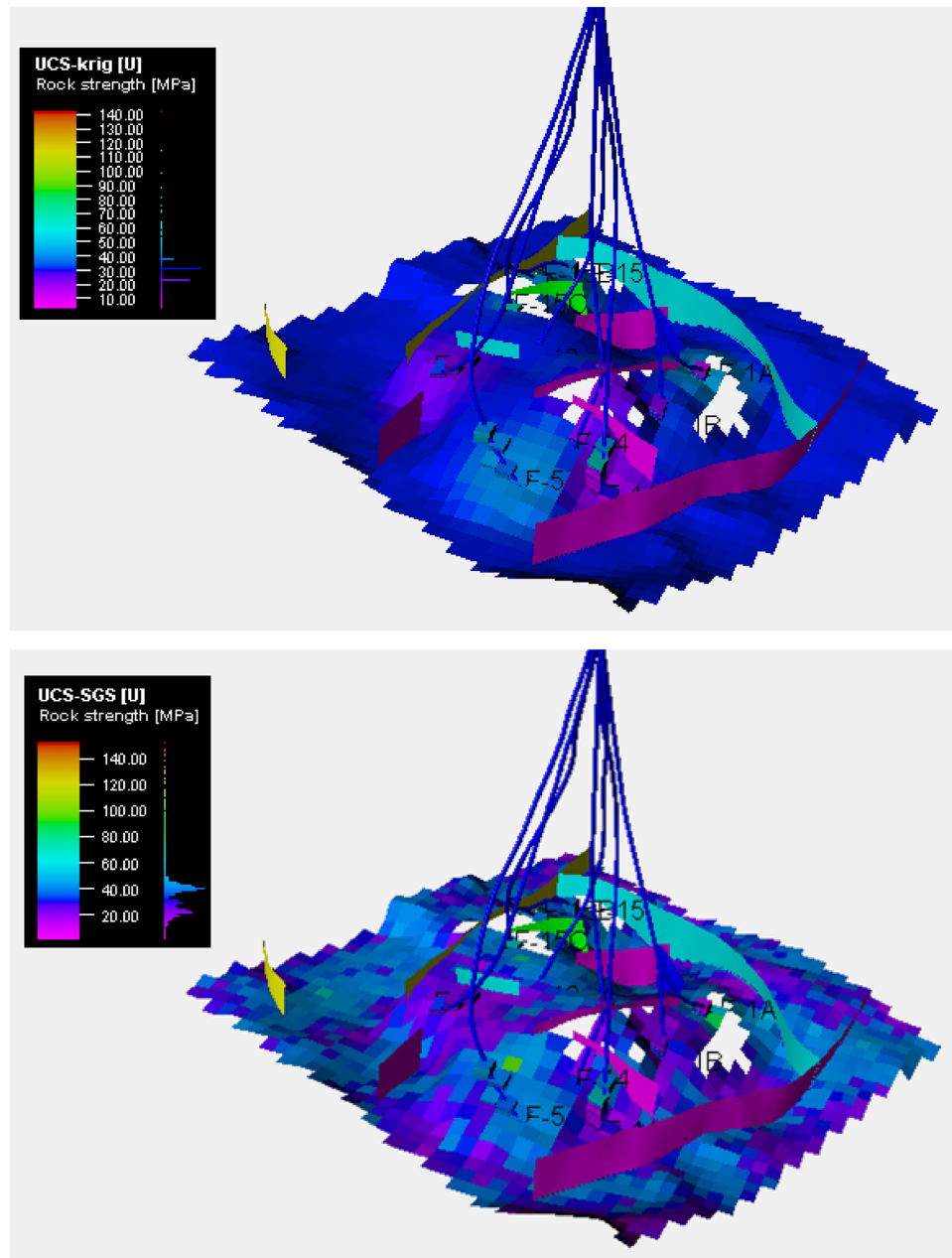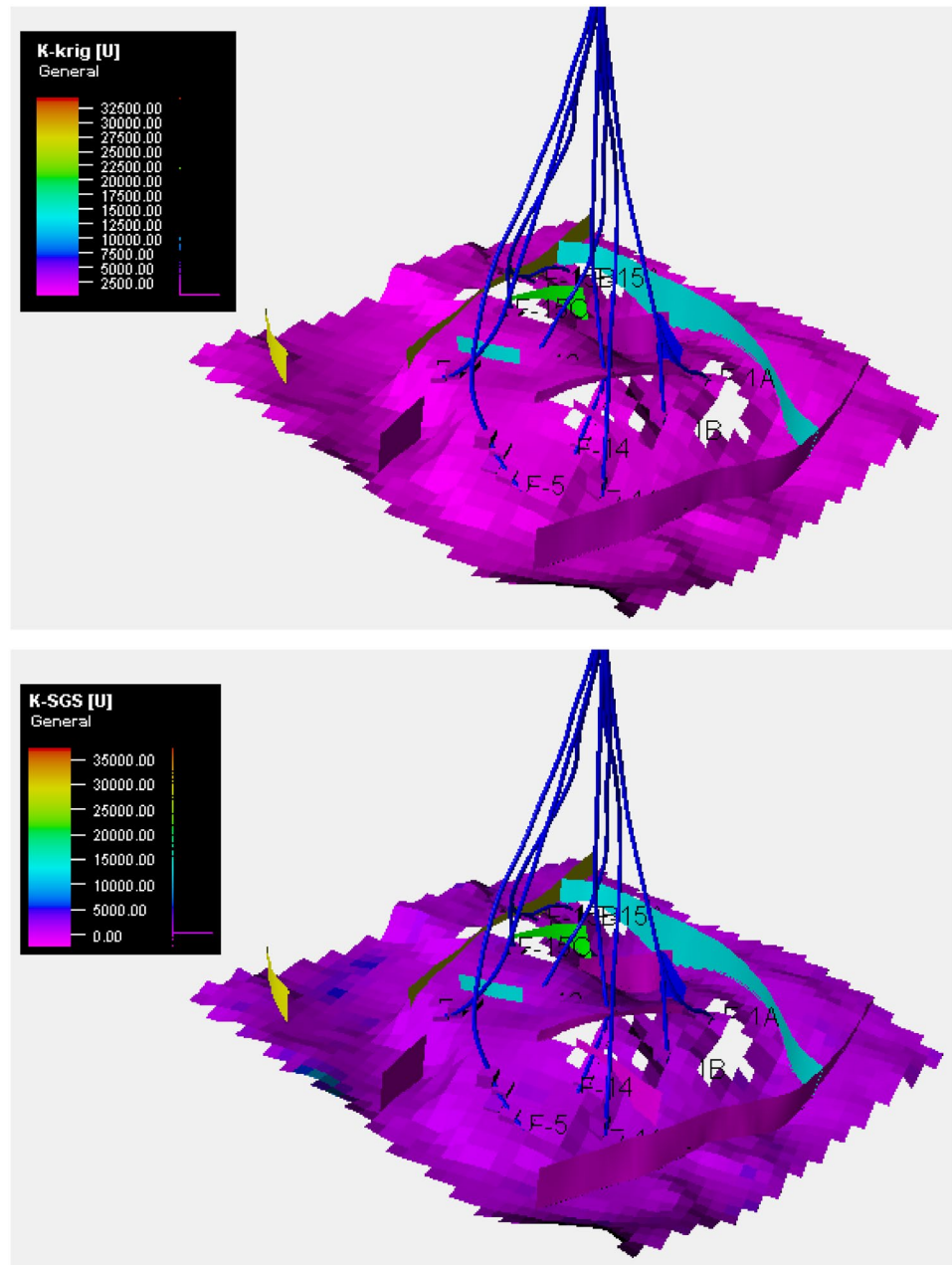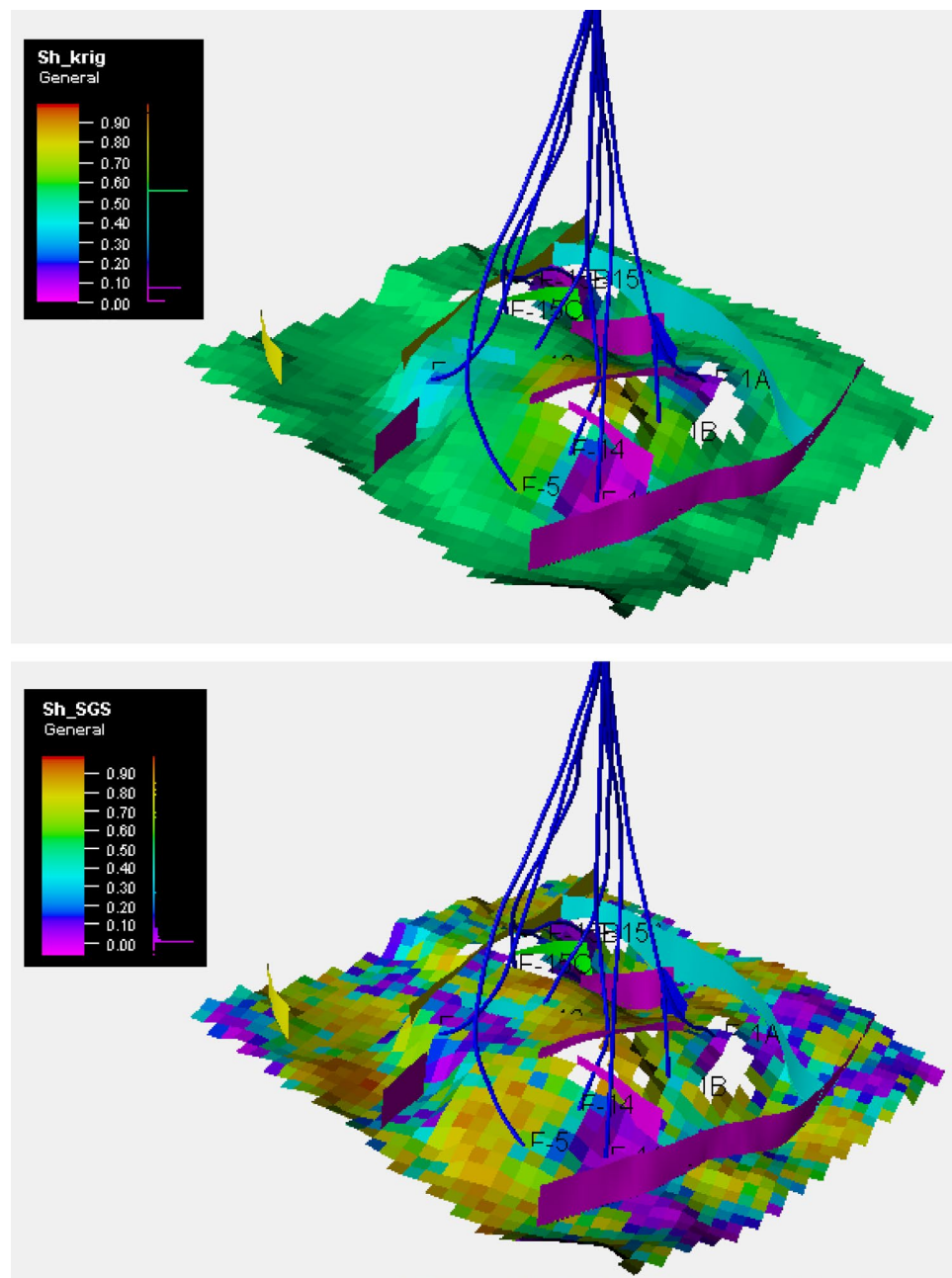
Fig. 17 Static UCS distribution through upscaled computed 1D well log properties: (top) Kriging (Krig) method and (bottom) SGS method

Appendix B Three-dimensional static reservoir modeling

The spatial distribution of the permeability and hydrocarbon saturation by using both Kriging and SGS methods are presented in Figs. 18 and 19, respectively.

Fig. 18 Static permeability distribution through upscaled computed 1D well log properties: (top) Kriging (Krig) method and (bottom) SGS method

Fig. 19 Static hydrocarbon saturation distribution through upscaled computed 1D well log properties: (top) Kriging (Krig) method and (bottom) SGS method

Declarations

Conflict of interest The authors have no conflicts of interest to declare that are relevant to the content of this article.

References

Adewunmi O, Adelu AA, Aderemi Adesoji O, Akanji Oluseun A, Sanuade SanLinn I, Kaka O, Afolabi S, Olugbemiga RO (2019) Application of 3D static modeling for optimal reservoir characterization. J Afr Earth Sc 152:184–196

Amanipoor H (2019) Static modeling of the reservoir for estimate oil in place using the geostatistical method. Geodesy and Cartograph 45(4):147–153. https://doi.org/10.3846/gac.2019.10386

Anees A, Zhang H, Ashraf U, Wang R, Liu K, Mangi HN, Shi W (2022a) Identification of favorable zones of gas accumulation via fault distribution and sedimentary facies: insights from Hangjinqi Area, Northern Ordos Basin. Front Earth Sci 9:1375. https://doi.org/10.3389/feart.2021.822670

Anees A, Zhang H, Ashraf U, Wang R, Liu K, Abbas A, Ullah Z, Zhang X, Duan L, Liu F, Zhang Y, Tan S, Shi W (2022b) Sedimentary facies controls for reservoir quality prediction of lower shihezi member-1 of the hangjinqi area. Ordos Basin Minerals 12:126. https://doi.org/10.3390/min12020126

Archer S, Rasouli V (2012) A log based analysis to estimate mechanical. petroleum and mineral resources, pp. 163–170.

Afsari M, Ghafoori M (2009) Mechanical earth model (MEM): An effective tool for borehole stability analysis and managed pressure drilling (case study). SPE Middle East Oil and Gas Show and Conference: OnePetro.

Ashraf U, Zhu P, Yasin Q, Anees A, Imraz M, Mangi HN, Shakeel S (2019) Classification of reservoir facies using well log and 3D seismic attributes for prospect evaluation and field development: a case study of Sawan gas field, Pakistan. J Petrol Sci Eng 175:338–351

Ashraf U, Zhang H, Anees A, Ali M, Zhang X, Shakeel Abbasi S, Nasir Mangi H (2020) Controls on reservoir heterogeneity of a shallow-marine reservoir in Sawan gas field, SE Pakistan: Implications for reservoir quality prediction using acoustic impedance inversion. Water 12(11):2972

Ashraf U, Zhang H, Anees A, Mangi HN, Ali M, Zhang X, Tan S (2021) A core logging, machine learning and geostatistical modeling interactive approach for subsurface imaging of lenticular geobodies in a clastic depositional system. SE Pakistan Natural Resour Res 30(3):2807–2830

Avseth P et al (2005) Quantitative seismic interpretation: applying rock physics tools to reduce interpretation risk. Cambridge University Press. https://doi.org/10.1017/CBO9780511600074

Bachmann G, Muller M, Weggen K (1987) Evolution of the Molasse Basin (Germany, Switzerland). Tectonophysics 137:77–92

Blanton TL, Olson JE (1999) Stress magnitudes from logs-effects of tectonic strains and temperature. SPE Reser Eval Eng 2(1):62–68

Bowers GL (1995) Pore pressure estimation from velocity data; accounting for overpressure mechanisms besides undercompaction. SPE Drilling and Completions. pp. 89–95.

Branets LV, Ghai SS, Lyons SL, Wu XH (2009) Challenges and technologies in reservoir modeling. Commun Comput Phys 6(1):1–23

Chambers RL, Yarus JM, Hird KB (2000) Petroleum geostatistics for nongeostaticians. Leading Edge J 19(6):592. https://doi.org/10.1190/1.1438664

Chopra S, Michelena RJ (2011) Introduction to reservoir characterization. Special edition of The Leading Edge, pp. 35–37.

Daines SR (1982) Prediction of fracture pressures for wildcat wells. J Petrol Technol 34(04):863–872

Davis JC (2002) Statistics and data analysis in geology. John Wilry & Sons.

Duran O, Sanei M, Devloo PRB, Santos ESR (2020) An enhanced sequential fully implicit scheme for reservoir geomechanics.

Comput Geosci 24(4):1557–1587. https://doi.org/10.1007/s10596-020-09965-2

Eaton BA (1968) Fracture gradient prediction and its application in oil field operations. In: SPE 43rd annual fall meeting, Houston, Texas, September 29–October 2, 25–32.

Eaton BA (1975) The Equation for Geopressure Prediction from Well Logs. Society of Petroleum Engineers of AIME. paper SPE 5544.

Equinor Website Database (2021) Available online: https://www.equinor.com/en/how-and-why/digitalisation-in-our-dna/volve-field-data-village-download.html (accessed on 9 July 2021).

Fischer K, Henk A (2013) A workflow for building and calibrating 3-D geomechanical models—A case study for a gas reservoir in the North German Basin. Solid Earth 4:347–355

Fjar E, Holt RM, Raaen A, Horsrud P (2008) Petroleum related rock mechanics. Elsevier

Flugel E (2004) Microfacies of carbonate rocks. Analysis, interpretation and application. Springer-Verlag, New York

Gardner GHF, Gardner LW, Gregory AR (1974) Formation velocity and density-the diagnostic basics for stratigraphic traps. Geophysics 39:770–780

Guerra C, Fischer K (2019) Henk A (2019) Stress prediction using 1D and 3D geomechanical models of a tight gas reservoir—A case study from the Lower Magdalena Valley Basin. Colombia Geomech Energy Environ 19:100113

Gutierrex M, Lewis RW (1998) The role of geomechanics in reservoir simulation. Paper Presented at the SPE/ISRM Rock Mech Petrol Eng, Trondheim, Norway. https://doi.org/10.2118/47392-MS

Henk A (2009) Perspectives of geomechanical reservoir models-why stress is important. Oil Gas Eur Mag 35:18–22

Herwanger J (2011) Seismic Geomechanics: How to Build and Calibrate Geomechanical Models using 3D and 4D Seismic Data. In Seismic Geomechanics: How to Build and Calibrate Geomechanical Models using 3D and 4D Seismic Data; European Association of Geoscientists and Engineers (EAGE): Houten, The Netherlands

Thanh HV, Sugai Y (2021) Integrated modelling framework for enhancement history matching in fluvial channel sandstone reservoirs. Upstream Oil Gas Technol 6:100027

Jiang R, Zhao L, Xu A, Ashraf U, Yin J, Song H, Anees A (2021) Sweet spots prediction through fracture genesis using multi-scale geological and geophysical data in the karst reservoirs of Cambrian Longwangmiao Carbonate Formation, Moxi-Gaoshiti area in Sichuan Basin, South China. Journal of Petroleum Exploration and Production Technology, pp.1–16.

Khaksar A, White A, Rahman K, Burgdor K, Ollarves R, Dunmore S (2012) Systematic geomechanical evaluation for short-term gas storage in depleted reservoirs. APPEA J 52:129–148

Kim M, Cha K, Lee TH, Choi DH (2002) Kriging interpolation methods in geostatistics and DACEModel. KSME Int J 16:619–632

Koutsabeloulis N, Xing Z (2009) 3D Reservoir geomechanical modeling in oil/gas field production. Paper Presented at the SPE Saudi Arabia Sect Tech Symposium, Al-Khobar, Saudi Arabia. https://doi.org/10.2118/126095-MS

Ma YZ (2011) Uncertainty analysis in reservoir characterization and management: how much should we know about what we don't know? In: Ma, Y.Z., La Pointe, P.R. (Eds.), Uncertainty Analysis and Reservoir Modeling: AAPG Memoir 96, pp. 1–15.

Mangi HN, Chi R, DeTian Y, Sindhu L, He D, Ashraf U, Anees A (2022) The ungrind and grinded effects on the pore geometry and adsorption mechanism of the coal particles. J Natural Gas Sci Eng, p. 104463.

Novak K, Malvik T, Velic J, Simon K (2014) Increased hydrocarbon recovery and CO2 storage in Neogene sandstones, a Croatian example: part II. Environ Earth Sci 71(8):3641–3653

Osinowo OO, Ayorinde JO, Nwankwo CP, Ekeng OM, Taiwo OB (2018) Reservoir description and characterization of Eni field offshore Niger Delta, southern Nigeria. J Petrol Explor Prod Technol 8(2):381–397. https://doi.org/10.1007/s13202-017-0402-7

Patrick DD, Gerilyn SS, John PC (2002) OutcropBase reservoir characterization: a composite Phylloid-Algal Mound, Western Orogrande Basin (New Mexico). AAPG Bull 86(1):780

Pereira LC, Guimarães LJN, FLO, Falcão (2008) Sensitivity Study of Geomechanical Effects on Reservoir Simulation. Australian Centre for Geomechanics, Perth. ISBN 978–0–9804185–5–2.

Plumb R, Edwards S, Pidcock G, Lee D, Stacey B (2000) The mechanical earth model concept and its application to high-risk well construction projects. In Proceed IADC/SPE Drill Conf, New Orleans, LA, USA 23–25:1–7

Plumb RA, Evans KF, Engelder T (1991) Geophysical log responses and their correlation with bed to bed stress contrasts in Paleozoic rocks, Appalachian plateau, New York. J Geophys Res 91:14509–14528

Safaei-Farouji M, Thanh HV, Dashtgoli DS, Yasin Q, Radwan AE, Ashraf U, Lee KK (2022) Application of robust intelligent schemes for accurate modelling interfacial tension of CO_2 brine systems: implications for structural CO_2 trapping. Fuel 319:123821

Sanei M, Duran O, Devloo PRB (2017) Finite element modeling of a nonlinear poromechanic deformation in porous media. In Proceedings of the XXXVIII Iberian Latin American Congress on Computational Methods in Engineering. ABMEC Brazilian Association of Computational Methods in Engineering. https://doi.org/10.20906/cps/cilamce2017-0418.

Sanei M, Duran O, Devloo PRB, Santos ESR (2021) Analysis of pore collapse and shear-enhanced compaction in hydrocarbon reservoirs using coupled poro-elastoplasticity and permeability. Arab J Geosci. https://doi.org/10.1007/s12517-021-06754-8

Sanei M, Duran O, Devloo PRB, Santos ESR (2022) Evaluation of the impact of strain-dependent permeability on reservoir productivity using iterative coupled reservoir geomechanical modeling. Geomech Geophys Geo-Energ Geo-Resour 8:54. https://doi.org/10.1007/s40948-022-00344-y

Schlumberger (2018) Techlog wellbore stability analysis workflow / solutions training.

Sen S, Ganguli SS (2019) Estimation of pore pressure and fracture gradient in Volve Field, Norwegian North Sea. SPE Oil and Gas India Conference and Exhibition, India, April.

Szydlik TJ, Way S, Smith P, Aamodt L, Friedrich C (2006) 3D PP/PS Prestack Depth Migration on the Volve Field. In Proceedings of the 68th EAGE Conference and Exhibition incorporating SPE EUROPEC, Vienna, Austria, pp. 12–15.

Tenthorey E, Vidal-Gilbert S, Backe G, Puspitasari R, Pallikathekathil Z, Maney B, Dewhurst D (2013) Modelling the geomechanics of gas reservoir: a case study from the Iona gas field. Australia Int J Greenh Gas Control 13:138–148

Tiab D, Donaldson EC (2015) Petrophysics: theory and Practice of Measuring Reservoir Rock and Fluid Transport Properties. Gulf professional publishing.

Vo Thanh H, Lee KK (2022) 3D geo-cellular modeling for Oligocene reservoirs: a marginal field in offshore Vietnam. J Petrol Explor Prod Technol 12:1–19. https://doi.org/10.1007/s13202-021-01300-4

Vo Thanh H, Sugai Y, Sasaki K (2020) Impact of a new geological modelling method on the enhancement of the CO_2 storage assessment of E sequence of Nam Vang field, offshore Vietnam. Energy Sources, Part a: Recovery, Utilization, and Environ Effects 42(12):1499–1512

Vo Thanh H, Yuichi S, Ronald N, Kyuro S (2019) Integrated workflow in 3D geological model construction for evaluation of CO_2 storage capacity of a fractured basement reservoir in Cuu Long Basin, Vietnam, International Journal of Greenhouse Gas Control, Volume 90.

Wang B, Sharma J, Chen J, Persaud P (2021) Ensemble machine learning assisted reservoir characterization using field production data–an offshore field case study. Energies 14:1052. https://doi.org/10.3390/en14041052

Yu XY, Ma YZ, Psaila D, Pointe PL, Gomez E, Li S (2011) Reservoir characterization and modeling: a look back to see the way forward. AAPG Mem 96:289–309

Zain-Ul-Abedin M, Henk A (2020) Building 1D and 3D mechanical earth models for underground gas storage—a case study from the molasse basin. Southern Germany Energies 13:5722. https://doi.org/10.3390/en13215722

Zhang J (2011) Pore pressure prediction from well logs: Methods, modifications, and new approaches. Earth Sci Rev 108(1–2):50–63

Zoback M, Moos D, Anderson R, Mastin L (1985) Wellbore breakouts and in situ stress. Geophys. J. p. 10.